CELL BIOLOGY

Lysosomal recycling of amino acids affects ER quality control

Ryo Higuchi-Sanabria[1]*, Koning Shen[1]*, Naame Kelet[1], Phillip A. Frankino[1], Jenni Durieux[1], Raz Bar-Ziv[1], Cierra N. Sing[2], Enrique J. Garcia[2], Stefan Homentcovschi[1], Melissa Sanchez[1], Rui Wu[1], Sarah U. Tronnes[1†], Larry Joe[1], Brant Webster[1], Alex Ahilon-Jeronimo[1], Samira Monshietehadi[1], Sofia Dallarda[1], Corinne Pender[1], Liza A. Pon[2], Roberto Zoncu[3], Andrew Dillin[1‡]

Recent work has highlighted the fact that lysosomes are a critical signaling hub of metabolic processes, providing fundamental building blocks crucial for anabolic functions. How lysosomal functions affect other cellular compartments is not fully understood. Here, we find that lysosomal recycling of the amino acids lysine and arginine is essential for proper ER quality control through the UPR^{ER}. Specifically, loss of the lysine and arginine amino acid transporter LAAT-1 results in increased sensitivity to proteotoxic stress in the ER and decreased animal physiology. We find that these LAAT-1–dependent effects are linked to glycine metabolism and transport and that the loss of function of the glycine transporter SKAT-1 also increases sensitivity to ER stress. Direct lysine and arginine supplementation, or glycine supplementation alone, can ameliorate increased ER stress sensitivity found in *laat-1* mutants. These data implicate a crucial role in recycling lysine, arginine, and glycine in communication between the lysosome and ER.

INTRODUCTION

Lysosomes play a critical role in cellular homeostasis by serving as the primary site of degradation through autophagy to provide essential resources for the cell (*1*–*4*). However, recent work has highlighted the role of the lysosome beyond a terminal degradative component. Instead, the lysosome has emerged as a central signaling hub of the cell, able to integrate multiple nutrient and stress signals to dynamically regulate cellular homeostasis (*5*). The signaling relationship between lysosomes and the endoplasmic reticulum (ER) is of particular interest because the lysosome serves primarily as a site for degradation of protein and lipids by autophagy, while the ER is a major site for protein and lipid synthesis. It is possible that there are interactions between the ER and lysosomes that coordinate their activities.

Similar to most organelle quality control, the relationship between the ER and lysosome is understood in the context of autophagic degradation of damaged organelles, or in this case "ER-phagy" (*6*). In ER-phagy, damaged ER are selectively degraded through autophagic mechanisms and delivered to the lysosome (*6*–*9*). However, these processes may require a particularly complex series of interactions between lysosomes and the damaged ER, because of the clear metabolic relationship between these two organelles. The first defense of ER health relies on the unfolded protein response (UPR^{ER}). Under conditions of ER stress, the UPR^{ER} activates several branches of ER quality control machineries, including ER-phagy, as well as transcriptional activation of chaperones, proteases, and other quality control factors (*10*, *11*). While the UPR^{ER} can trigger autophagy in numerous ways [reviewed in (*12*)], how lysosomal function and quality can alter the UPR^{ER} and ER homeostasis beyond ER-phagy and in the context of nutrient signaling is not well understood. Through large-scale RNA interference (RNAi) screening of lysosomal genes, we identified LAAT-1, an exporter of the amino acids lysine and arginine from the lysosome, as a regulator of ER homeostasis through coordination of lysosomal amino acid recycling. Through additional screening of known amino acid transporters, we also identified SKAT-1, a glycine transporter, in functioning in a similar manner to LAAT-1 in regulating ER homeostasis.

RESULTS

RNAi screening of lysosomal genes reveals LAAT-1 as a regulator of the UPR^{ER}

We performed an RNAi-based screen in *Caenorhabditis elegans* to identify lysosomal genes required for proper ER quality control (Fig. 1A). Specifically, we performed knockdown of ~600 lysosomal genes and tested their impact on UPR^{ER} induction under conditions of ER stress. ER stress was applied by inhibiting N-linked glycosylation of proteins using two methods: (i) chemical inhibition by the drug tunicamycin and (ii) inhibition by RNAi knockdown of *tag-335*, a gene essential for N-linked glycosylation of proteins in the ER. UPR^{ER} induction was measured using a transcriptional reporter, where green fluorescent protein (GFP) expression is driven under the promoter of *hsp-4* (*hsp-4p::GFP*), a direct target of XBP-1s which is highly up-regulated under conditions of ER stress (*13*). The level of GFP expression serves as a qualitative and semiquantitative measure of UPR^{ER} induction. Through this screening effort, we identified several lysosomal genes that either suppress or enhance stress-induced UPR^{ER} (Fig. 1A).

We found that RNAi knockdown of only one specific gene, *laat-1*, resulted in a robust increase in stress-induced UPR^{ER} using both chemical and genetic means (Fig. 1, A to C). We validated our screen finding using a previously characterized hypomorphic mutant, *laat-1(qx42)*, which phenocopies RNAi knockdown (Fig. 1, D and E) (*14*). Moreover, the increased UPR^{ER} induction is not specific to

[1]Department of Molecular and Cellular Biology, Howard Hughes Medical Institute, The Glenn Center for Aging Research, University of California, Berkeley, Berkeley, CA 94720-3370, USA. [2]Department of Pathology and Cell Biology, Columbia University, New York, NY 10032, USA. [3]Department of Biochemistry, Biophysics, and Structural Biology, University of California, Berkeley, Berkeley, CA 94720-3370, USA.
*These authors contributed equally to this work.
†Present address: Department of Molecular, Cell, and Developmental Biology, University of Colorado Boulder, Boulder, CO 80309, USA.
‡Corresponding author. Email: dillin@berkeley.edu

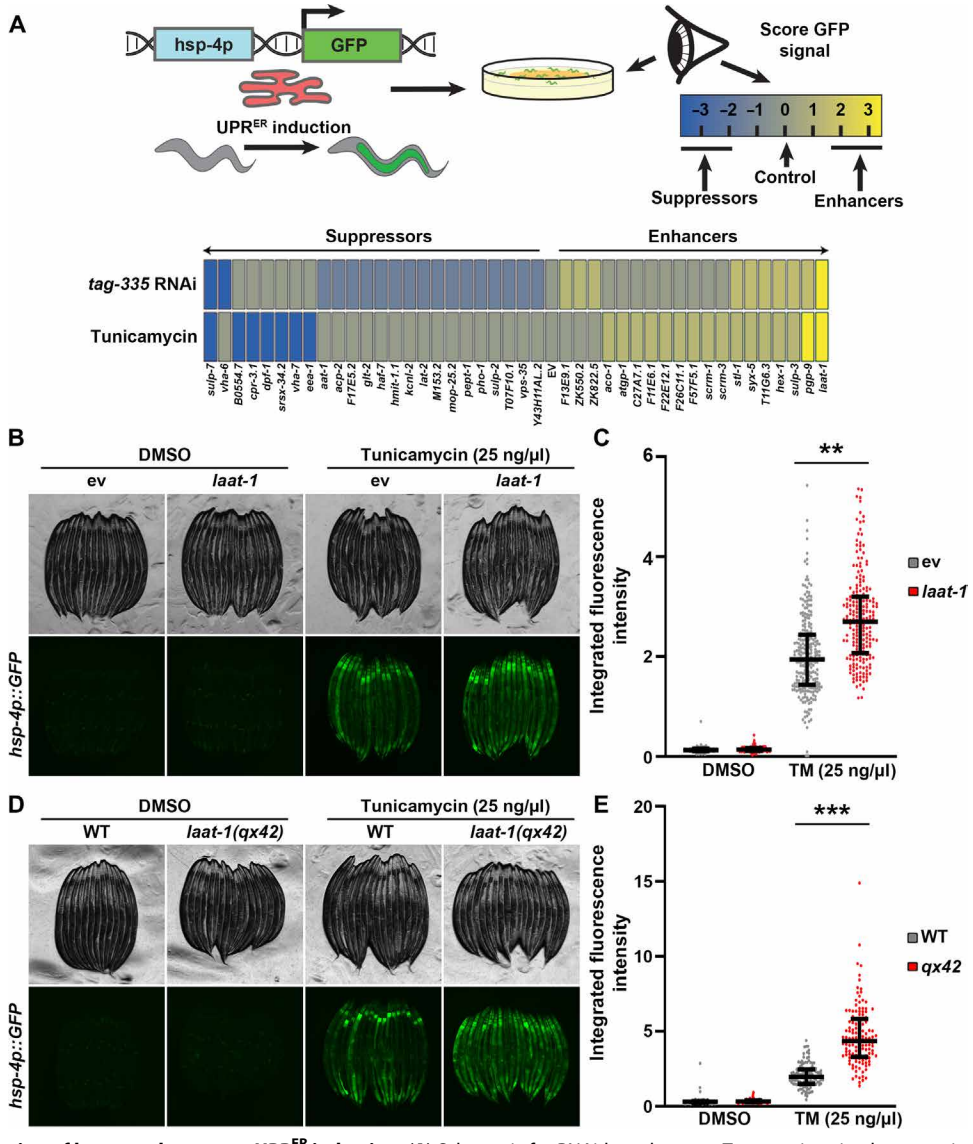

Fig. 1. RNAi-based screening of lysosomal genes on UPR^{ER} induction. (**A**) Schematic for RNAi-based screen. Transgenic animals expressing *hsp-4p::GFP* were grown on either tunicamycin (25 ng/μl) or *tag-335* RNAi, as described in Materials and Methods. Animals were scored qualitatively by eye for either suppression or enhancement of the *hsp-4p::GFP* induction compared to *hsp-4p::GFP* animals on empty vector RNAi control. Suppressors are shown in blue on the left, and enhancers are shown in yellow on the right. Intensity of color indicates level of suppression or enhancement. (**B**) Fluorescent micrographs of *hsp-4p::GFP* animals grown on control (ev) or *laat-1* RNAi from hatch. Animals are treated with 1% dimethyl sulfoxide (DMSO) or tunicamycin (25 ng/μl), as described in Materials and Methods. Data are representative of four independent trials. (**C**) Quantification of (B) using a biosorter. $^{**}P < 0.01$ using Mann-Whitney testing. Each dot represents a single animal, middle line represents median, and whiskers represent interquartile range. $n = 219$ to 224 per strain. (**D**) Fluorescent micrographs of WT or *laat-1(qx42)* animals with *hsp-4p::GFP* animals grown on HT115 bacteria from hatch. Animals are treated with 1% DMSO or tunicamycin (25 ng/μl), as described in Materials and Methods. Data are representative of four independent trials. (**E**) Quantification of (D) using a biosorter. $^{***}P < 0.001$ using Mann-Whitney testing. Each dot represents a single animal, middle line represents median, and whiskers represent interquartile range. $n = 122$ to 134 animals per strain.

inhibition of N-linked glycosylation by tunicamycin or *tag-335* knockdown, as *laat-1(qx42)* animals also exhibit increased UPR^{ER} induction through RNAi knockdown of *sec-11*, a serine peptidase, and through lipid dysregulation by *sbp-1* RNAi (fig. S1, A to D). Because *hsp-4* is a transcriptional target of XBP-1s, we next tested whether the enhanced activation of the UPR^{ER} in *laat-1* RNAi-treated or mutant animals was dependent on *xbp-1s*. We find that RNAi knockdown of *xbp-1s* fully suppresses the UPR^{ER} induction in *laat-1(qx42)* animals, similar to wild-type (WT) controls (fig. S1, E and F). Moreover, we find that *laat-1(qx42)* animals have a much higher level of *xbp-1s* transcripts under ER stress compared to WT controls (fig. S2A). Last, to confirm that loss of *laat-1* results in a broad increase in XBP-1s–mediated UPR^{ER} induction, we performed RNA sequencing (RNA-seq) analysis on *laat-1* loss-of-function animals compared to WT animals. We find that in *laat-1* mutants, there is an up-regulation of XBP-1s targets when treated with tunicamycin in comparison to WT controls (fig. S2B).

To determine whether the regulation of ER homeostasis through lysosome-derived amino acids was specific to lysine and arginine, we performed a screen of all characterized amino acid transporters,

including those not directly associated with the lysosome. We find that knockdown of three additional transporters increased tunicamycin-induced UPR^{ER} similar to *laat-1* loss of function: *skat-1, slc-36.2*, and *F13H10.3* (fig. S3A). F13H10.3 is predicted to be functionally similar to SLC38A9, which acts as a lysosomal arginine sensor downstream of mammalian target of rapamycin (mTOR) signaling, thus having a functionally similar role to LAAT-1 and corroborating our findings (*15*). SKAT-1 and SLC36.2 are predicted to be functionally similar to SLC36A1, which has functions in transporting glycine and alanine (*16*). We find that glycine supplementation alone can increase UPR^{ER} induction under stress. However, *laat-1* knockdown and glycine supplementation do not have an additive effect on tunicamycin sensitivity, suggesting that glycine and LAAT-1 may affect ER stress sensitivity through a similar mechanism (Fig. 2). To determine that this was not a phenomenon shared by all amino acids in general, we also supplemented *laat-1* loss-of-function animals with glutamic acid, which had no effect on UPR^{ER} induction in either WT or *laat-1* loss-of-function animals (Fig. 2). These data suggest that glycine, lysine, and arginine are uniquely important in ER homeostasis.

Of the two predicted homologs to SLC36A1, SKAT-1 localizes to the lysosome and regulates lysosomal function, potentially through TOR2 (*17*). Moreover, loss of *skat-1* and *laat-1* independently resulted

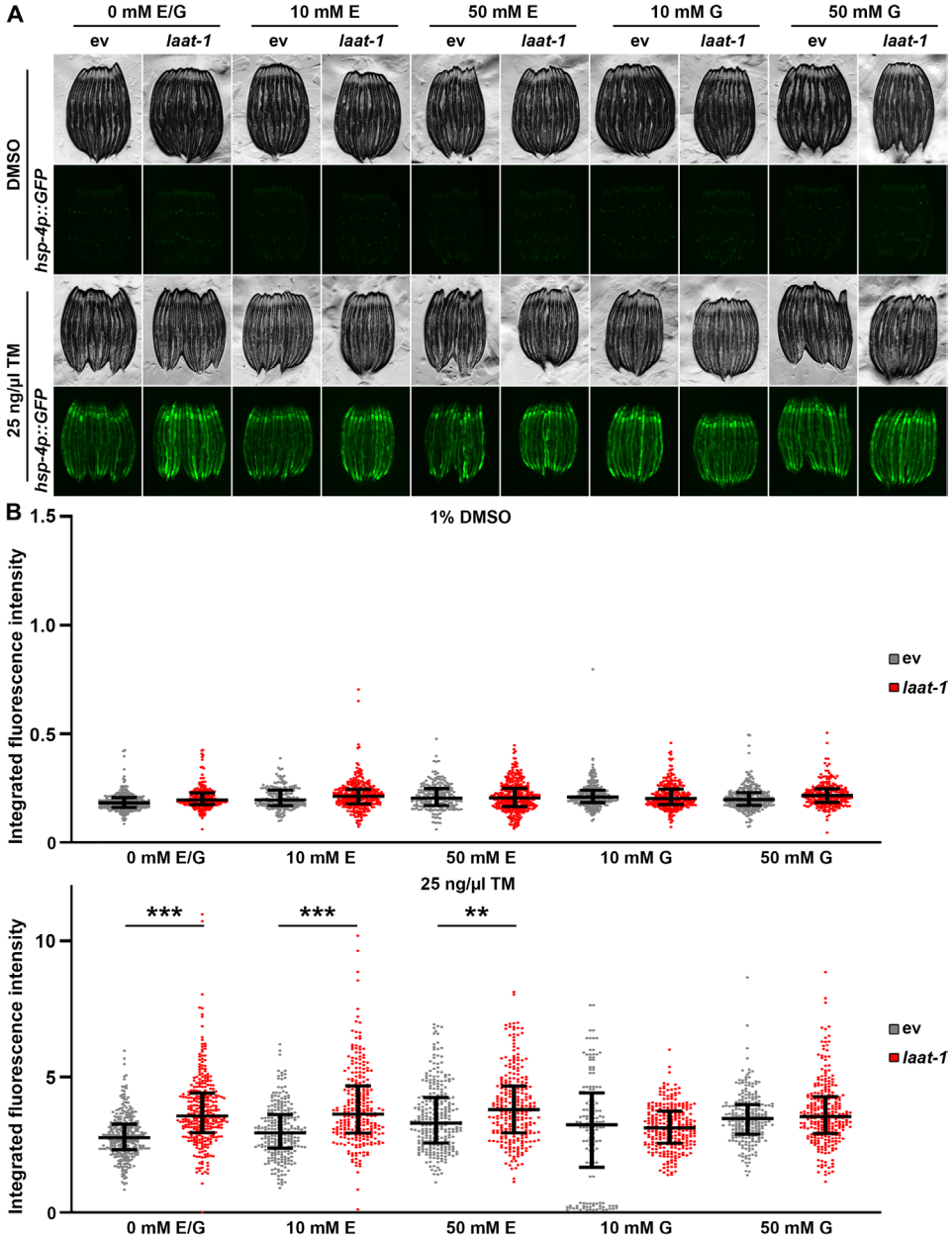

Fig. 2. Glycine supplementation rescues ER stress sensitivity of *laat-1* loss-of-function animals. (**A**) Fluorescent micrographs of *hsp-4p::GFP* animals grown on control (ev) or *laat-1* RNAi plates supplemented with 0, 10, or 50 mM glutamic acid (E) or glycine (G) from hatch. Animals are treated with 1% DMSO or tunicamycin (25 ng/µl), as described in Materials and Methods. Data are representative of three independent trials. (**B**) Quantification of (A) using a biosorter. ***$P < 0.001$ and **$P < 0.01$ using Mann-Whitney testing. Each dot represents a single animal, middle line represents median, and whiskers represent interquartile range. $n = 202$ to 428 animals per condition.

in a similar increase in UPR^{ER} activation under ER stress (fig. S3, B and C). Therefore, we tested whether LAAT-1 or SKAT-1 functioned in similar or distinct and independent mechanistic pathways in ER homeostasis. Simultaneous knockdown of *skat-1* and *laat-1* did not have an additive effect, and animals with knockdown of both exhibit similar UPR^{ER} induction compared to either *laat-1* or *skat-1* knockdown alone (fig. S3, B and C). These data suggest that *laat-1* and *skat-1* function in similar molecular pathways in the regulation of ER homeostasis.

laat-1 loss of function results in increased sensitivity to ER stress and decreased organismal health

We continued to characterize the functional implications of *laat-1* loss of function. We asked whether the observed *laat-1* enhancement of UPR^{ER} signaling is protective or detrimental to ER health. While induction of UPR^{ER} is generally used as a marker of stress, ectopic activation of UPR^{ER} in the absence of ER stress can also be beneficial. For example, overexpression of *xbp-1s* results in increased UPR^{ER} activation, increased resistance to ER stress, and increased life span by promoting ER protein homeostasis (*18*). Here, we find that loss of *laat-1* results in animals that exhibit a notable decrease in life span and increased sensitivity to ER stress through tunicamycin (Fig. 3, A to D). Moreover, these animals exhibit a substantial decrease in motility when exposed to acute or chronic tunicamycin treatment, suggesting that health span is compromised when exposed to ER stress (Fig. 3, E and F). Last, *laat-1* loss-of-function animals exhibit a severely disordered ER morphology, including decreased tubular networks and organization of the ER (Fig. 4). In addition, tunicamycin treatment caused the ER to completely fragment into indistinguishable aggregates in animals lacking *laat-1*, compared to much less severe fragmentation in WT animals (Fig. 4). These data suggest that the increased UPR^{ER} activation in animals lacking *laat-1* is not beneficial and may be the result of increased sensitivity of these animals to ER stress.

Because animals lacking *laat-1* exhibit increased sensitivity to ER stress, we sought to determine whether animals lacking *laat-1* also increased UPR^{ER} induction in the absence of stress. Overexpression of *xbp-1s* results in ectopic activation of UPR^{ER}, bypassing the need

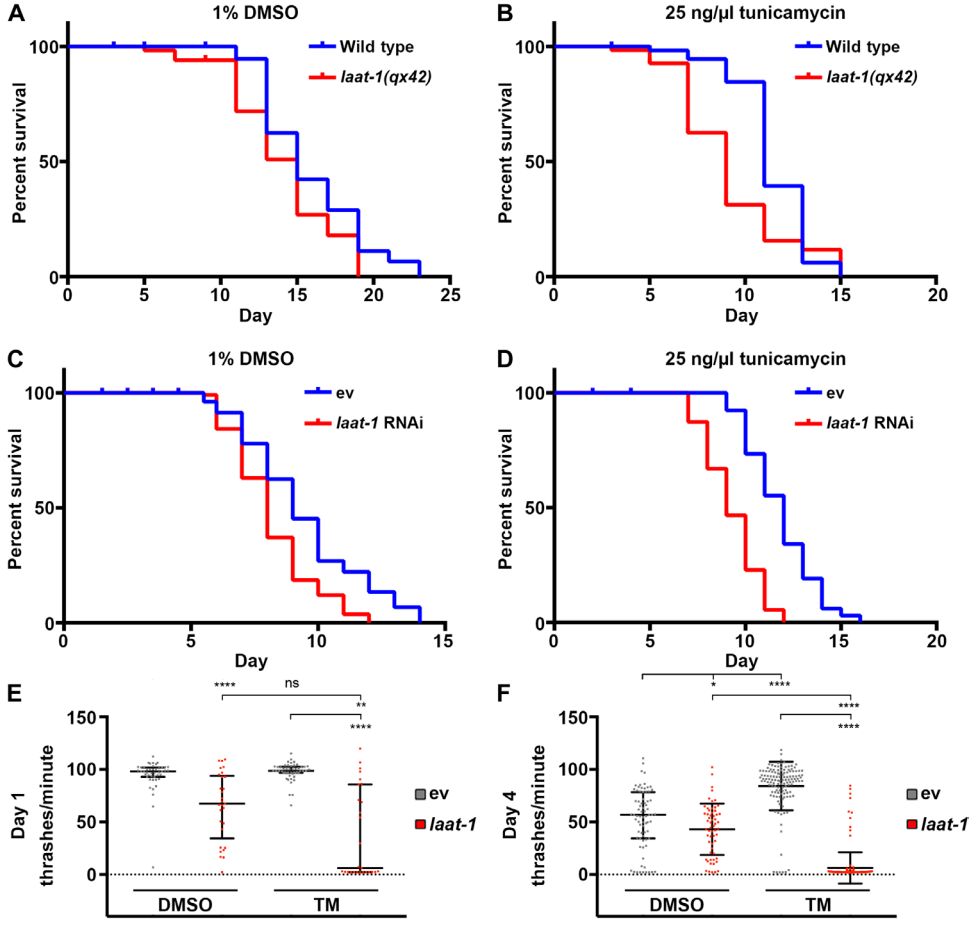

Fig. 3. *laat-1* loss-of-function animals have increased sensitivity to ER stress. (**A** and **B**) Life spans of WT control or *laat-1(qx42)* animals grown on either 1% DMSO (A) or tunicamycin (25 ng/µl) (B), as described in Materials and Methods. Data are representative of three independent trials. See table S1 for statistics. (**C** and **D**) Life spans of WT animals grown on control (ev) or *laat-1* RNAi from hatch and on either 1% DMSO (C) or tunicamycin (25 ng/µl) (D), as described in Materials and Methods. Data are representative of three independent trials. See table S1 for statistics. (**E** and **F**) Thrashing was measured in WT animals grown on either ev or *laat-1* RNAi from hatch, exposed to either 1% DMSO or tunicamycin (25 ng/µl) (TM) for 1 (E; day 1) or 4 (F; day 4) days. Data are representative of two independent trials. $^{**}P < 0.01$ and $^{****}P < 0.0001$ using Mann-Whitney testing. Each dot represents a single animal, middle line represents median, and whiskers represent interquartile range. $n = 27$ to 50 per strain for day 1, and 58 to 160 per strain for day 4.

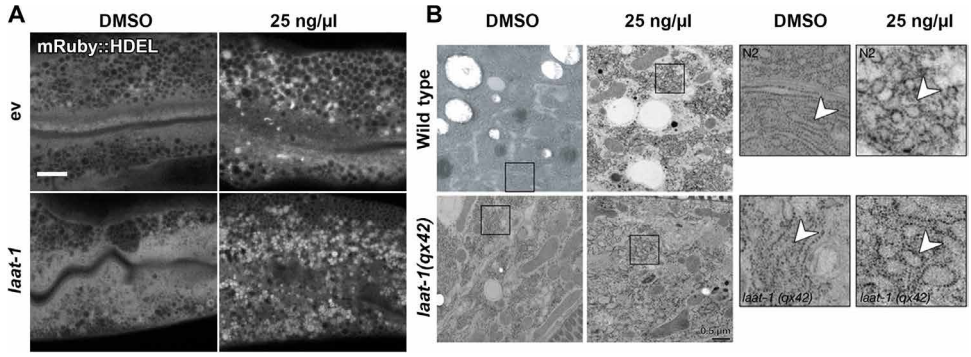

Fig. 4. *laat-1* loss-of-function animals exhibit defects in ER morphology. (**A**) Representative micrographs of ER morphology [using *hsp-4* signal sequence fused to mRuby::HDEL, the signal sequence allows mRuby to be imported into the matrix of the ER, while the HDEL serves as a sequestration signal (*40*)]. This marker is reliably used for robust ER imaging in the intestine of animals grown on control (ev) or *laat-1* RNAi from hatch. Animals were pretreated with 1% DMSO or tunicamycin (25 ng/μl), as described in Materials and Methods. Scale bar, 10 μm. Data are representative of three independent trials. (**B**) Electron micrographs of intestine from WT control and *laat-1(qx42)* animals at D1 of adulthood. Animals were pretreated with 1% DMSO or tunicamycin (25 ng/μl), as described in Materials and Methods. Boxed areas are of ER morphology zoomed in at the right of the image. Arrowheads indicate ER structures.

to expose animals to stress for UPR^{ER} induction (*18*). Similar to previous studies, we find that overexpression of *xbp-1s* specifically in the intestine or systemically across all cells strongly induces UPR^{ER}. In contrast to UPR^{ER} activation upon stress, loss of *laat-1* function does not affect UPR^{ER} induction via *xbp-1s* overexpression, providing further evidence that *laat-1* increases sensitivity to ER stress, rather than general augmentation of UPR^{ER} induction (fig. S4). It is also possible that *laat-1* acts upstream of *xbp-1* splicing; thus, overexpression of *xbp-1s* bypasses *laat-1* function.

Because animals lacking *laat-1* exhibit gross perturbations in lysosomal function (*14*) and lysosomes are essential for general quality control through autophagic clearance of damaged cellular components (*19*), it is possible that these animals exhibit a general increase in stress sensitivity. Therefore, we tested whether loss of *laat-1* resulted in increased sensitivity to mitochondrial stress through RNAi knockdown of *cco-1*, a mitochondrial cytochrome c oxidase; heat stress through exposure to elevated temperature; or oxidative stress through paraquat (PQ) treatment. We used similar reporters to *hsp-4p::GFP* as a marker for these stresses and found that *laat-1* RNAi knockdown did not affect induction of the UPR of the mitochondria (UPR^{MT}; *hsp-6p::GFP* reporter) or the heat shock response (HSR; *hsp-16.2p::GFP* reporter) (fig. S5, A and B). However, loss of *laat-1* did increase sensitivity of animals to oxidative stress (*gst-4p::GFP* reporter) (fig. S5C). Recent work uncovered that intracellular lysine concentrations may regulate oxidative stress response by affecting glutathione levels (*20*). It is possible that loss of *laat-1* increases ER stress sensitivity due to decreased cytoplasmic lysine pools and ultimately decreased glutathione levels and poor redox handling. Therefore, we tested the impact of knockdown of the rate-limiting step in glutathione synthesis, *gcs-1*, on UPR^{ER} induction. In contrast to *laat-1* RNAi knockdown animals, *gcs-1* RNAi knockdown animals did not exhibit increased UPR^{ER} induction under ER stress, suggesting that increased ER stress sensitivity in animals lacking *laat-1* is likely not due to decreased glutathione levels (fig. S5D). To directly test whether loss of *laat-1* affects redox homeostasis in the ER, we used an ER-localized redox-sensitive GFP variant, eroGFP, to measure the redox state of the ER in the budding yeast model *Saccharomyces cerevisiae* (*21*, *22*). We find that yeast cells harboring a deletion of *YPQ1* [yeast homolog of *laat-1* (*23*)] exhibit no change in eroGFP under basal conditions. *ypq1*Δ cells do not exhibit poor redox handling, as changes in eroGFP through exposure to reducing stress [dithiothreitol (DTT)] or oxidizing stress (H_2O_2) were similar in *ypq1*Δ and WT cells (fig. S6). Therefore, we conclude that *laat-1* loss of function does not result in a general sensitivity to ER-specific oxidative stress. More likely, ER homeostasis is disrupted in *laat-1* loss-of-function animals and these animals are more sensitive to general oxidative stress or have activated oxidative stress response pathways as a downstream effect of increased ER stress. Previous work has shown that perturbing ER homeostasis may result in activation of a noncanonical oxidative stress response through SKN-1 activity (*24*).

Because *laat-1* plays a central role in amino acid transport of the lysosome, we tested whether general loss of lysosomal function could phenocopy the effects of *laat-1* loss. To perturb general lysosomal function, we performed RNAi knockdown of subunits of the v-ATPase (vacuolar-type H^+ adenosine triphosphatase), a critical enzyme that acidifies the lysosomal lumen (*25*, *26*). We find that knockdown of *vha-7*, which did not affect animal growth, had no impact on UPR^{ER} induction under stress. Knockdown of *vha-13*, which results in severe growth defects of animals, did increase UPR^{ER} induction under stress. However, loss of *laat-1* markedly increased sensitivity to ER stress for animals with knockdown of either *vha-7* or *vha-13* (fig. S7, A and B), suggesting that *laat-1* phenotypes are not dependent on the loss of lysosomal acidity. Similarly, we find that loss of *laat-1* also increased UPR^{ER} induction even upon RNAi knockdown of the lysosomal biogenesis factor, *hlh-30*, the *C. elegans* TFEB homolog (fig. S7, C and D). These data suggest that the loss of *laat-1* does not increase ER sensitivity through the maintenance of lysosomal acidification or general lysosomal stress signaling. However, we find that blocking autophagy via knockdown of *bec-1*, the *C. elegans* homolog of beclin-1, did partially suppress the increased UPR^{ER} induction of animals lacking *laat-1*, suggesting that the increase in ER sensitivity is at least partially dependent on functional autophagy (fig. S7, C and D).

laat-1 regulates ER homeostasis through recycling of lysine and arginine

Through autophagy, lysosomes play a critical role in recycling essential building blocks within the cell. Specifically, LAAT-1 functions

as an exporter of lysosomal arginine and lysine (*14*). Therefore, we wondered whether the loss of *laat-1* results in increased ER stress due to the lack of recirculating lysine and arginine. To test this hypothesis, we performed amino acid supplementation of lysine and arginine in animals lacking *laat-1*. We find that 10 and 50 mM lysine and arginine supplementation suppressed the increase in UPR^{ER} induction in animals lacking *laat-1*, with 50 mM lysine and arginine supplementation showing stronger suppression (Fig. 5, A and B, and fig. S8). Moreover, 10 mM lysine and arginine supplementation partially suppressed the morphological defects of the ER of animals lacking *laat-1* (Fig. 5C). Last, 10 mM lysine and arginine supplementation partially rescued the life-span defect and full restoration of the ER stress sensitivity of these animals (Fig. 5, D and E). These data provide evidence that LAAT-1 plays a critical role in ER

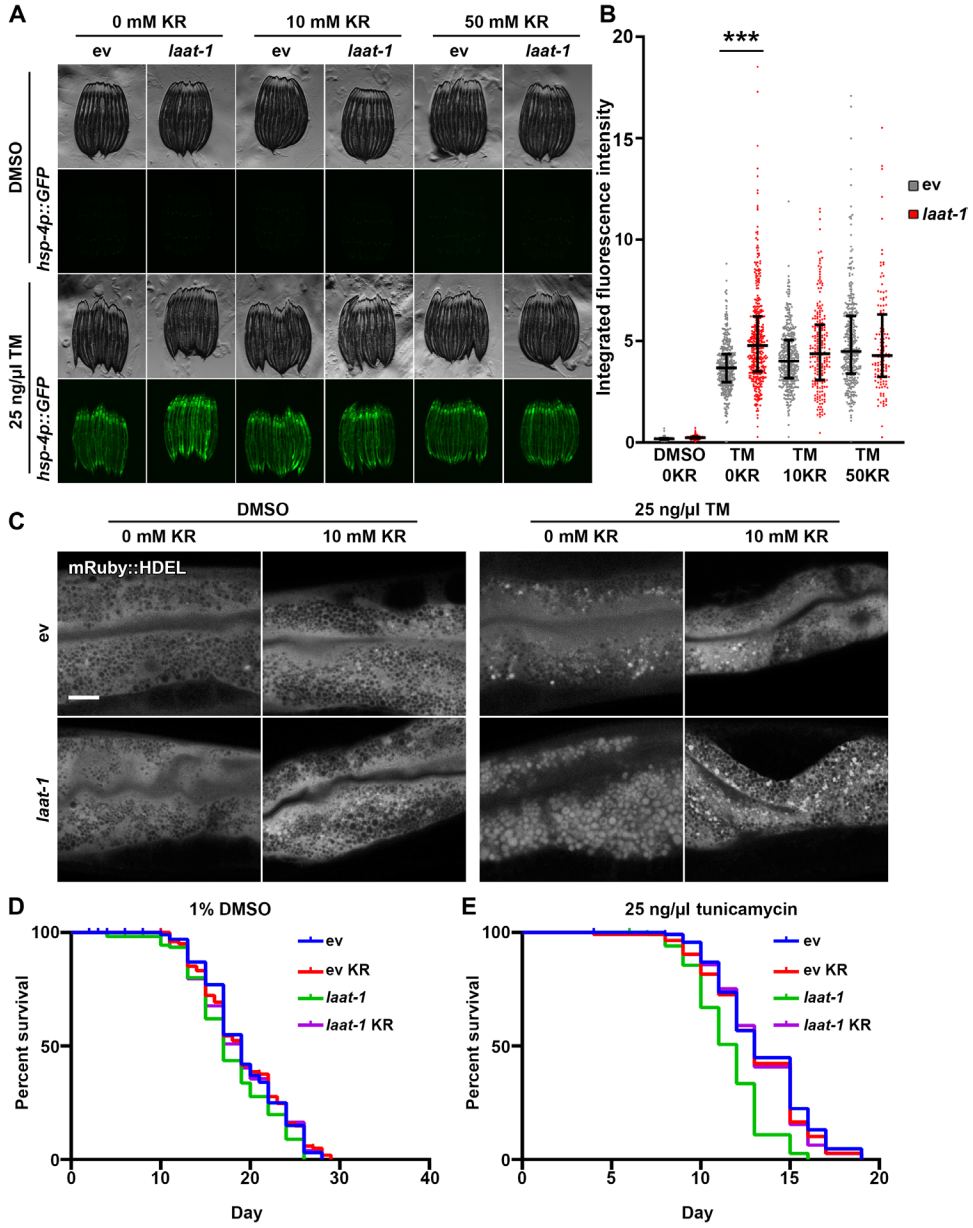

Fig. 5. Lysine and arginine supplementation is sufficient to rescue defects in ER homeostasis of *laat-1* loss-of-function animals. (**A**) Fluorescent micrographs of *hsp-4p::GFP* animals grown on control (ev) or *laat-1* RNAi plates supplemented with 0, 10, or 50 mM lysine/arginine (KR) from hatch. Animals are treated with 1% DMSO or tunicamycin (25 ng/µl), as described in Materials and Methods. Data are representative of three independent trials. (**B**) Quantification of (A) using a biosorter for DMSO 0KR, TM 0KR, TM 10KR, and TM 50KR. Full panel of quantification is shown in fig. S6. ***$P < 0.001$ using Mann-Whitney testing. Each dot represents a single animal, middle line represents median, and whiskers represent interquartile range. $n = 101$ to 366 per strain. (**C**) Representative micrographs of ER morphology in the intestine of animals grown on control (ev) or *laat-1* RNAi plates supplemented with 10 mM lysine/arginine (KR) from hatch. Animals were pretreated with 1% DMSO or tunicamycin (25 ng/µl), as described in Materials and Methods. Scale bar, 10 µm. Data are representative of three independent trials. (**D** and **E**) Life spans of WT animals grown on control (ev) or *laat-1* RNAi from hatch and on either 1% DMSO (D) or tunicamycin (25 ng/µl) (TM) (E) supplemented with 10 mM lysine/arginine (KR), as described in Materials and Methods. Data are representative of four independent trials. See table S1 for statistics.

homeostasis and organismal health under proteotoxic stress. Moreover, lysosomal arginine and lysine transport through LAAT-1 plays at least some functional role in life-span regulation.

Last, because there are other key nutrients recycled and sensed at the lysosome, we asked whether altered general nutrient sensing through *laat-1* played a role in the enhanced UPR^{ER} stress signal. Nutrient sensing, particularly of amino acids, is primarily performed by the mTOR complex (mTORC) and GCN2 (*15*, *27*, *28*). mTOR directs cellular growth under rich nutrient conditions, and its regulation is tightly linked to the availability of growth factors and amino acids, particularly arginine and leucine (*29*). mTORC1 activation relies on this amino acid sensing via the Ragulator complex at the surface of the lysosome (*28*, *30*, *31*). GCN2 senses uncharged transfer RNAs (tRNAs), which accumulate as a result of limited amino acid availability and promotes the integrated stress response to downregulate global translation (*32*). To test whether the loss of *laat-1* activates these starvation signals, we performed RNAi knockdown of *gcn-2* and *let-363* (CeTOR, *C. elegans* mTORC ortholog). We find that loss of *laat-1* increased UPR^{ER} activation in *gcn-2* knockdown animals similar to that observed in the empty vector control. We find that RNAi knockdown of *let-363* further increased UPR^{ER} activation of animals lacking *laat-1*. These data suggest that LAAT-1 signaling through lysine and arginine to maintain ER homeostasis is independent of GCN2 but synergistic with mTORC signaling (fig. S9, A and B). Last, to test whether the effects of the loss of *laat-1* is due to decreased lysine and arginine, or just an effect of general starvation, we tested the impact of animals to starvation on sensitivity to ER stress. Starvation in WT animals did not affect UPR^{ER} induction under ER stress. However, in animals lacking *laat-1*, starvation had a markedly additive effect on UPR^{ER} induction, similar to the synergistic effect seen with mTOR knockdown (fig. S9, C and D). These data suggest that specific recycling of lysine and arginine through LAAT-1, and not just general starvation, is especially critical to ER homeostasis.

DISCUSSION

To identify a novel relationship between lysosomal activity and ER protein homeostasis, we performed a large-scale RNAi-based screen to identify lysosomal genes that regulate UPR^{ER} signaling. We found that loss of function of the lysosomal amino acid transporter LAAT-1 results in potent enhancement of UPR^{ER} activation under conditions of stress. Our data indicate that this increased UPR^{ER} signaling is a sign of increased sensitivity to ER stress and not an increased protective response. Loss of *laat-1* results in the breakdown of the ER under proteotoxic stress, decreased life span, and increased sensitivity of these animals to ER stress. This is not due to general lysosomal dysfunction but is specific to the loss of export of recycled lysine and arginine out from the lysosome. Last, reintroduction of glycine can rescue defects in *laat-1* loss-of-function animals, suggesting a parallel pathway in ER homeostasis, potentially through the glycine transporter *skat-1* (Fig. 6).

Still to be identified is how cellular depletion of lysine, arginine, and glycine can disrupt ER homeostasis. Here, we show that the phenotypes associated with loss of function of *laat-1* are partially dependent on autophagy. Moreover, another study has shown that depletion of arginine in human immune cells leads to an ER stress response involving activation of autophagy as a cytoprotective mechanism (*33*). Last, PQLC2, the mammalian homolog of *laat-1*, has been shown to be involved in lysine and arginine export (*34*). Therefore, it is possible that depletion of LAAT-1/PQLC2 could cause a dysfunction in autophagy, which creates a low level of ER stress that is only measurable upon further ER stress. *laat-1* loss-of-function animals only have mild defects in growth but exhibit a major increase in sensitivity to ER stress. Moreover, they have reduced life span, which suggests that the mild level of cellular stress they experience exacerbates aging phenotypes, another phenomenon that is closely linked to reduced autophagy (*19*).

Another plausible mechanism is that the available pool of lysine and arginine has an impact on ER homeostasis independent of autophagy. It is possible that deprivation of these essential amino acids affects ER quality and/or function directly or that impinging on general nutrient sensing pathways perturbs ER homeostasis. Here, we find that knockdown of CeTOR and starvation phenocopied *laat-1* knockdown and increased ER stress sensitivity. However, both of these phenotypes were additive with *laat-1*, which suggest that *laat-1* and starvation signals act in mechanistically distinct pathways such that simultaneous loss of both results in additive effects. Alternatively,

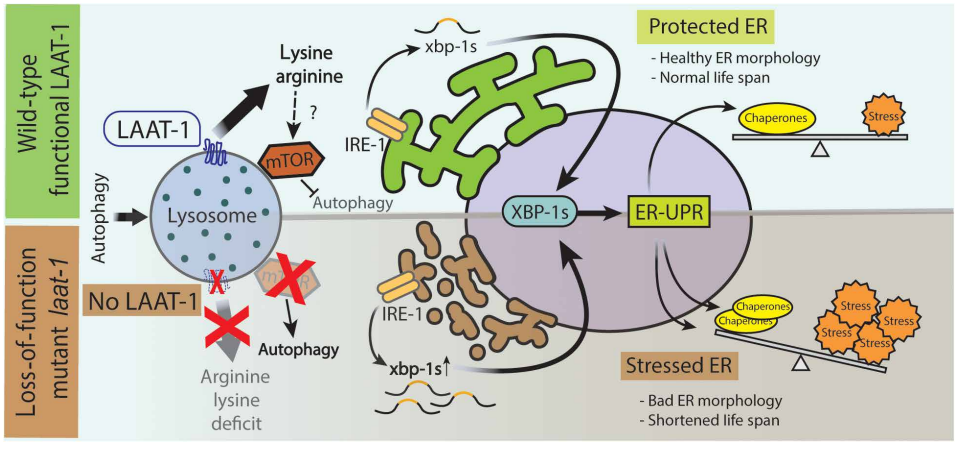

Fig. 6. LAAT-1 modulates ER homeostasis through recycling of lysine and arginine. Lysosomal amino acid recycling of lysine and arginine, potentially via autophagy, is essential for proper ER quality control. *laat-1* mutants exhibit increased sensitivity to ER stress, increase UPR^{ER} activation, have severe defects in ER morphology, and suffer from decreased survival under ER proteotoxic stress. Lysine and arginine supplementation rescues suggest that LAAT-1 regulates ER homeostasis by recycling lysine and arginine. These phenotypes are partially dependent on mTOR and autophagy.

because the starvation experiments performed here were for only 2 hours and CeTOR was inhibited by RNAi knockdown, it is possible that there was only partial inhibition of TOR through these methods. Thus, loss of function of LAAT-1 could potentially further inhibit TOR beyond starvation or RNAi knockdown, resulting in a synergistic effect on the same molecular pathway. This latter hypothesis is appealing, as recent work has ascribed mTOR function in deactivating IRE1 upon UPR activation to prevent prolonged UPR^{ER} that could potentially be detrimental (*35*). In this model, TOR inhibition would result in sustained and prolonged UPR^{ER}, which could lead to cellular damage. Thus, it is likely that we see increased UPR^{ER} activation under stress in *laat-1* knockdown animals due to sustained UPR^{ER} activation upon inhibition of TOR.

Overall, our data indicate a unique role for lysosomal recycling of amino acids on ER homeostasis under stress and suggest that there may be a specific role for lysine and arginine in ER homeostasis. These phenotypes may be driven by the role of LAAT-1 in lysosomal regulation of nutrient availability, particularly of lysine and arginine amino acids, which have downstream implications on autophagy and TOR signaling. Moreover, the role of SKAT-1 in lysosomal recycling of glycine also contributes to ER homeostasis, implicating lysosomal lysine, arginine, and glycine in ER homeostasis.

MATERIALS AND METHODS

Strains and maintenance

All *C. elegans* strains are derivatives of N2 from Caenorhabditis Genetics Center (CGC) and are listed in table S2. All worms were grown at 15° to 20°C on nematode growth medium (NGM) agar plates and fed OP50 *Escherichia coli* B strain of bacteria for general maintenance. For experimentation, all animals were grown on HT115 *E. coli* K12 strain of bacteria carrying the pL4440 empty vector control or expressing double-stranded RNA containing the sequence of the target gene. All experiments were performed on animals synchronized using a standard bleaching/L1 arresting protocol. Briefly, animals were harvested from NGM plates with M9 solution (22 mM KH_2PO_4 monobasic, 42.3 mM Na_2HPO_4, 85.6 mM NaCl, and 1 mM $MgSO_4$), bleached using a solution of 1.8% sodium hypochlorite and 0.375 M KOH diluted in dH_20 until all carcasses are digested, intact eggs were washed four times with M9 solution, and worms were grown in M9 solution for ~12 to 16 hours rotating in a 15-ml conical tube at 20°C to L1 arrest. Animals were grown to desired developmental stage on HT115 bacteria or RNAi bacteria.

For lysine and arginine experiments, plates were supplemented with 10 or 50 mM lysine and arginine buffered with HCl to pH 7.0. Animals are grown on lysine/arginine supplemented plates from hatch and for the duration of the entire experiment.

All *S. cerevisiae* strains are derivatives of the WT BY4741 strain from Open Biosystems and are listed below. Yeast cells were cultivated in synthetic complete (SC) media with corresponding dropouts of essential nutrients for auxotrophic selection. All imaging experiments were carried out with cultures grown to mid-log phase [OD_{600} (optical density at 600 nm) = 0.1 to 0.3] in a 30°C shaking incubator. *ypq1Δ* strain was created by replacing the *YPQ1* gene locus with *hphMX4* using a standard lithium acetate transformation method. Polymerase chain reaction (PCR) using specific primers (5′-TTCACTACGTACTTTAATCGTCTTCGCGA-3′ and 5′-TTTGTGACATTAAAAAAATGTCAATGACAGAGAGA-3′) were used to confirm deletion of the gene. eroGFP and UPR-RFP (red fluorescent protein) reporter was amplified from plasmid pPM56 (a gift from F. Papa, Addgene plasmid no. 22855; RRID: Addgene_22855) and cloned into HO-polyKanMX4-HO (a gift from D. Stillman, Addgene plasmid no. 51662; RRID: Addgene_51662) using Sal I and Bgl II (*36*, *37*). Last, the cassette HO-eroGFP-UPR-RFP-HO was inserted in the HO locus of a WT strain to generate eroGFP UPR strain using the standard lithium acetate transformation method.

ypq1 deletion primers are the following (for pCY 3090-02, hygro): 5′-TACAAAAAAAAAGCTACCACATCGCTCGACGACCTCAATTCGGATCCCCGGGTTAATTAA-3′ and 5′-GAGGTCAAAAATATGTTAAATAAATATTAGATAGAACATGATCGATGAATTCGAGCTCG-3′.

Primers to clone eroGFP-UPR marker into HO locus are the following: 5′-GCGCGTCGACGAGCTCCACCGCGGAGTTTA-3′ and 5′-GCGCAGATCTAGGTCGACGGTATCGATAAGCTT-3′.

Primers to integrate at HO locus are the following: 5′-GCCGCCAGCTGAAGCTTAATTAT-3′ and 5′-CATAGGCCACTGTAAGATTCCGCC-3′.

Biosorter analysis

Staged worms were washed off plates using M9. A Union Biometrica complex object parameter analyzer and sorter (COPAS) biosorter (product no. 350-5000-000) equipped with a 561-nm and 488-nm light source was used for imaging. Biosorter calibration, cleaning, and sample running were performed as previously described (*38*). Analysis is performed in Excel and represented as integrated intensity of fluorescence normalized to the size of the animal measured as the product of extinction (approximate width) and time of flight (approximate length). All data that exceed the measurement capacity of the PMT (photomultiplier tube) (i.e., saturated signals) and bad profiles (curved worms, bent worms, etc.) determined as described in (*38*) were removed from analysis.

Confocal microscope

To fix worms, day 1 adults are collected using M9 solution and excess bacteria are washed three times with M9 (do not exceed ~1000g; 1000 RCF (relative centrifugal force) on an Eppendorf centrifuge 5702). Animals were treated with 1% dimethyl sulfoxide (DMSO) or tunicamycin (25 ng/μl) diluted in M9 solution spinning in a 15-ml conical tube at 20°C for 4 hours. Animals were then pelleted, excess M9 is aspirated down to 100 μl, and an equal volume of 4% buffered paraformaldehyde (PFA) was added directly to worms [4% PFA in 1% phosphate-buffered saline (PBS)]. Tubes were rotated in a 20°C incubator. PFA is washed three times using 1% PBS and placed into 70% glycerol buffered in 1% PBS overnight to rehydrate. For imaging, glycerol samples are mounted directly on glass slides, covered with a coverslip, and sealed with nail polish. Fixed animals were viewed on a Zeiss LSM700 inverted confocal microscope. Figure images are single slices focused at the central plane of the intestine equidistant from the vulva and tail.

Electron microscopy

Whole worm samples were processed as previously described (*39*). Briefly, staged animals were subject to high-pressure freezing (BALTEC HPM 010) and freeze-substituted with acetone/resin series (25%-50%-75%-100% resin). Resin-cured worms were sectioned into 70-nm sections and imaged using an FEI Tecnai 12 transmission electron microscope on formvar-coated mesh grids. Animals were treated with either 1% DMSO or tunicamycin (25 ng/μl) by moving

synchronized L4 animals onto NGM plates containing 1% DMSO or tunicamycin (25 ng/μl) for 12 to 16 hours to image at D1 adulthood.

Epifluorescence microscopy

Staged worms are picked at random under a white light microscope and immobilized in 100 nM sodium azide. Immobilized worms were aligned on a solid NGM plate, and images were captured on a Leica M250FA stereoscope equipped with a Hamamatsu ORCA-ER camera driven by LAS-X software.

For *hsp-4p::GFP* induction, synchronized L4 animals were treated with a solution of tunicamycin (25 ng/μl), 1% DMSO, 100 μM thapsigargin, or 10 mM DTT, diluted in M9 solution for 4 hours spinning at 20°C in a 15-ml conical tube (note that bacteria are not clarified after washing animals off plates to minimize starvation during the treatment). Animals were then washed three times with M9 and placed on a standard OP50 plate to recover for 12 to 16 hours before imaging. For *tag-335* and *sec-11* RNAi, animals were grown from L1 until D1 adulthood on RNAi and imaged at D1. For starvation experiments, animals were washed four times in M9 to clarify bacteria and were left spinning in M9 in 15-ml conical tubes at 20°C for 2 hours. Animals are then spun with a solution of tunicamycin (25 ng/μl) in M9 without bacteria for a total of 6 hours of starvation. Animals were then placed on a standard OP50 plate for 12 to 16 hours before imaging.

For *hsp-4p::GFP* screening, animals were grown from hatch until D1 adulthood using two methods: (i) For chemical induction of *hsp-4p::GFP*, animals were grown on standard RNAi plates from hatch until L4, then washed and moved onto equivalent RNAi plates containing tunicamycin (25 ng/μl) for 24 hours, and imaged at D1 adulthood, and (ii) for genetic induction of *hsp-4p::GFP*, animals were grown on standard RNAi plates from hatch and imaged at D1 adulthood—animals were grown on 10% *tag-335* RNAi mixed with 90% RNAi of interest.

For *hsp-6p::GFP* induction, animals were grown from L1 until D1 adulthood on *cco-1* RNAi and imaged at D1. RNAi treatment is 50% *cco-1* mixed with 50% RNAi of interest based on OD_{600}.

For *hsp-16.2p::GFP* induction, D1 animals were heat-shocked for 2 hours at 34°C and recovered for 2 hours at 20°C before imaging.

For *gst-4p::GFP* induction, synchronized L4 animals were treated with a 50 mM PQ solution diluted in M9 for 2 hours spinning at 20°C in a 15-ml conical tube. Animals were then washed three times with M9 and placed on a standard OP50 plate to recover for 2 hours before imaging.

Wide-field microscopy

Images were acquired with an Axioskop 2 microscope equipped with an Orca-ER cooled CCD (charge-coupled device) camera (Hamamatsu) and a pE-4000 LED (light-emitting diode) illumination system (coolLED, Andover, UK) controlled by NIS-Elements 4.60 Lambda software (Nikon, Melville, NY). For drug treatments, mid-log phase cells were treated with 2 mM DTT for 30-min shaking at 30°C and imaged immediately. For H_2O_2, cells were treated with 10 mM H_2O_2 for 30-min shaking at 30°C, H_2O_2 was washed out with SC, and then animals were recovered for 3-hour shaking at 30°C before imaging. Cell suspension (1.5 μl) was applied to a microscope slide and covered with a coverslip. Cells were imaged immediately after mounting using a 100×/1.4 Plan Apochromat objective (Carl Zeiss), 405- and 470-nm LEDs at 100% power for excitation of oxidized and reduced forms, respectively, and a modified GFP filter (Zeiss filter set 46 HE with excitation filter removed; dichroic FT 515, emission 535/30).

Images of eroGFP were collected with Z-series throughout the entire cell at 0.3-μm intervals using 1 × 1 binning and 150- and 300-ms exposures for 470 and 405 nm, respectively. Images were deconvolved using a constrained iterative restoration algorithm with the following parameters: 507-nm excitation wavelength, 60 iterations over 100% confidence in Volocity (PerkinElmer, Waltham, MA). To calculate the reduced to oxidized ratio, the intensity of the reduced channel was divided by the intensity of the oxidized channel, with ratioing performed in Volocity software including background selection and thresholding steps.

Life-span analysis

Life-span measurements were performed on solid NGM agar plates, with HT115 bacteria carrying either pL4440 empty vector or RNAi. Worms were synchronized by standard bleaching-L1 arresting and kept in 20°C throughout the duration of the experiment. Adult worms were moved away from progeny onto fresh plates for the first 7 days until progeny were no longer visible and then scored every 1 to 2 days until all animals were scored. Animals with bagging, vulval explosions, or other age-unrelated deaths were censored and removed from quantification. For tunicamycin survival assays, animals are moved onto tunicamycin (25 ng/μl) or 1% DMSO plates at D1 of adulthood.

Thrashing measurements

Health span was measured in worms using thrashing. Animals were grown on solid NGM agar plates with HT115 bacteria carrying either pL4440 empty vector or *laat-1* RNAi. Worms were synchronized by standard bleaching-L1 arresting and kept in 20°C until the L4 stage. L4 animals were either moved onto NGM agar plates containing either 1% DMSO or tunicamycin (25 ng/μl), seeded with their respective RNAis. Animals were moved away from progeny onto fresh DMSO/tunicamycin plates daily until thrashing assays were performed on either day 1 or day 4. To measure thrashing, aged animals were washed from the plate with M9 and rinsed once with M9 to remove excess bacteria. Worm/M9 mix was then transferred onto an NGM plate without bacteria and recovered on the plate for 30 s before imaging. Worms were then recorded using an MBF Bioscience WormLab worm tracker for 30 s. Thrashing rate (also referred to in the analysis software as "wave initiation rate") was analyzed using the "swimming" analysis mode in WormLab for the 30-s recorded interval, excluding animals that were tracked for <15 s.

RNA-seq and qPCR analysis

Animals were synchronized and grown to D1 of adulthood on EV RNAi plates. About 2000 animals were harvested using M9, and animals were treated with either 1% DMSO or tunicamycin (25 ng/μl) in M9 solution, spinning at 20°C for 1 hour in a 15-ml conical tube. After an hour of treatment, M9 was aspirated and replaced with Trizol, and worms were freeze/thawed three times with liquid nitrogen/37°C water bath cycles. After the final thaw, chloroform was added at a 1:5 ratio of chloroform:Trizol. Aqueous separation of RNA was performed via centrifugation using a heavy gel phase-lock tube (VWR, 10847-802). The aqueous phase was mixed with isopropanol, and then RNA purification was performed using the Qiagen RNeasy Mini Kit as per the manufacturer's directions. Library preparation was performed using Kapa Biosystems mRNA Hyper Prep Kit. Sequencing was performed using Illumina HS4000, mode

SR100, through the Vincent J. Coates Genomic Sequencing Core at University of California, Berkeley.

For quantitative PCR (qPCR), complementary DNA (cDNA) synthesis was performed using the Qiagen QuantiTect Reverse Transcription Kit (Qiagen, 205311) on 2 μg of RNA as per the manufacturer's guidelines. qPCR was performed using a general standard curve protocol using SYBR Select Master Mix (Life Technologies, 4472920). A master mix of all cDNA samples pooled with equal ratios was used as a template for the standard curve for each primer pair. Four technical replicates were performed for two independent biological replicates per sample. The following primer pairs were used, written as 5′ to 3′ orientation and forward/reverse primer: *hsp-4*, GAACAACCTACTCGTGCGTTGG/TTGATCTCCGGAAAACGCAACG; *crt-1*, ATGACGAGATGGACGGAGAAT/CTGACTTGACCTGCCACAAAT; *xbp-1*, CACCTCCATCAACAACAACAT/AACCGTCTGCTCCTTCCTCAA; and *xbp-1s*, CGTGCCTTTGAATCAGCAGTG/CGAGGTGTCCATCTTCTTGTT. The following genes were used as housekeeping genes, and a calculated geometric mean of all replicates from all genes was used for normalization for each sample: *pmp-3*, TGGCCGGATGATGGTGTCGC/ACGAACAATGCCAAAGGCCAGC; *tba-1*, TCAACACTGCCATCGCCGCC/TCCAAGCGAGACCAGGCTTCAG; and *Y45F10D.4*, CGAGAACCCGCGAAATGTCGGA/CGGTTGCCAGGGAAGATGAGGC.

For RNA-seq, analysis was performed on the CLC Workbench version 7.0.3. Mapping was performed using the *C. elegans* reference genome and transcript sequence from Ensembl/WormBase (PR513758.WS273). Unique reads were calculated for each library. All data were normalized for the different number of reads for each library, and a factor of 0.01 was added to each expression value and transformed by $\log_2$. Two biological replicates were compiled per each treatment comparison to run EDGE (empirical analyses of digital gene expression) testing to provide significantly up- or down-regulated genes per sample. For this article, XBP-1s targets were identified using the following Gene Ontology (GO) terms from BioMart WormBase ParaSite: 0006990, 0030968, 0036498, and 1900101. The $\log_2$(foldchange) of N2 tunicamycin versus N2 DMSO and *laat-1(qx42)* tunicamycin versus *laat-1(qx42)* DMSO was calculated for each of these targets.

Statistics and rigor of experiments

The full lysosome library screen was performed once per condition (tunicamycin treatment and *tag-335* RNAi) by two independent researchers. Only hits that were independently scored identically by both researchers were included. All hits were validated at least two more times by independent researchers.

All imaging experiments were performed with at least three independent trials unless otherwise stated in the figure legends. All animals picked for experiments are performed blinded on a standard dissection microscope without fluorescent capability to ensure robust reproducibility. Quantification on a biosorter was performed with a large sample size on at least one of the three imaging replicates per experiment. Prism 8 software was used for nonparametric Mann-Whitney statistical testing for biosorter data.

All life spans were performed with at least three independent trials unless otherwise stated in the figure legends. Replicates were performed by at least two independent researchers, with minimally one replicate performed with the researcher blinded to sample conditions to ensure robust reproducibility. Prism 8 software was used for statistical analysis using log-rank (Mantel-Cox) testing.

Synthesis of *laat-1* RNAi *pL4440-laat-1*

laat-1 RNAi was synthesized by Sma I restriction digest of pL4440 followed by restriction digest–based cloning with a 558–base pair sequence of *laat-1* (AGCCAATTCAAAAGATTATTGGCGTTTATTATATTATACAGGATCTCGTTCTATGGACACAATATGGATATTATCTGAAGATTTATAATAGACCTACCACGTCATCAGCGCGTTCCAACACAATCGTTGTACCCGTACTCGCATTGGCATCAGTCGGATCATTTTTCGTGTTTGAATCGGCTCTGCCACCTGTTGGAGATCATCGAGTTAAGCGCTCTTTCCTGGAGTCACTAAACCATCAAGAAGGTCTCCCACTGGAAGGAATTCTTAAAATGTGGCCAATTTTCACGTCGTACACTGATATGCTTGGTTATATAATTGGATCGATGGCCGCTGTTTGCTATTTCGGTGGAAGAATTCCCCAAATTATCAAAAACTACCGGCATTCTTCGTGTGAAGGACTCTCGTTGACCATGTTCTACATTATTGTCGCTGCCAATTTTACTTACGGGATCTCTGTGCTATTGGCAACGACTAGTTGGCTTTATTTGTTGAGACATCTCCCATGGTTGGCTGGAAGTCTCGGCTGCTGCTGCTTCGACGCTGTAATCATCTCTC) synthesized via PCR using forward primer ACGTGACGCGTGGATCCCCCAGCCAATTCAAAAGATTATTGGCG and reverse primer ATATCGAATTCCTGCAGCCCGAGAGATGATTACAGCGTCGAAG. Ligation was performed using T4 DNA ligase following standard protocol and was transformed into HT115 *E. coli* K12 bacteria. Knockdown efficiency was tested via qPCR (~80% knockdown efficiency) using forward primer GCTTCGACGCTGTAATCATCTCTC and reverse primer CTAATCGGAGTCGTCTTGTGAATTGAG.

SUPPLEMENTARY MATERIALS

Supplementary material for this article is available at http://advances.sciencemag.org/cgi/content/full/6/26/eaaz9805/DC1

View/request a protocol for this paper from *Bio-protocol*.

REFERENCES AND NOTES

1. J. A. Martina, H. I. Diab, O. A. Brady, R. Puertollano, TFEB and TFE3 are novel components of the integrated stress response. *EMBO J.* **35**, 479–495 (2016).
2. C. L. Nezich, C. Wang, A. I. Fogel, R. J. Youle, MiT/TFE transcription factors are activated during mitophagy downstream of Parkin and Atg5. *J. Cell Biol.* **210**, 435–450 (2015).
3. N. Raben, R. Puertollano, TFEB and TFE3: Linking lysosomes to cellular adaptation to stress. *Annu. Rev. Cell Dev. Biol.* **32**, 255–278 (2016).
4. T. Tsunemi, T. D. Ashe, B. E. Morrison, K. R. Soriano, J. Au, R. A. V. Roque, E. R. Lazarowski, V. A. Damian, E. Masliah, A. R. L. Spada, PGC-1α rescues huntington's disease proteotoxicity by preventing oxidative stress and promoting TFEB function. *Sci. Transl. Med.* **4**, 142ra97 (2012).
5. R. M. Perera, R. Zoncu, The lysosome as a regulatory hub. *Annu. Rev. Cell Dev. Biol.* **32**, 223–253 (2016).
6. A. Khaminets, T. Heinrich, M. Mari, P. Grumati, A. K. Huebner, M. Akutsu, L. Liebmann, A. Stolz, S. Nietzsche, N. Koch, M. Mauthe, I. Katona, B. Qualmann, J. Weis, F. Reggiori, I. Kurth, C. A. Hübner, I. Dikic, Regulation of endoplasmic reticulum turnover by selective autophagy. *Nature* **522**, 354–358 (2015).
7. S. Schuck, C. M. Gallagher, P. Walter, ER-phagy mediates selective degradation of endoplasmic reticulum independently of the core autophagy machinery. *J. Cell Sci.* **127**, 4078–4088 (2014).
8. S. A. Houck, H. Y. Ren, V. J. Madden, J. N. Bonner, M. P. Conlin, J. A. Janovick, P. M. Conn, D. M. Cyr, Quality control autophagy degrades soluble ERAD-resistant conformers of the misfolded membrane protein GnRHR. *Mol. Cell* **54**, 166–179 (2014).
9. P. Grumati, G. Morozzi, S. Hölper, M. Mari, M.-L. I. Harwardt, R. Yan, S. Müller, F. Reggiori, M. Heilemann, I. Dikic, Full length RTN3 regulates turnover of tubular endoplasmic reticulum via selective autophagy. *eLife* **6**, e25555 (2017).
10. P. Walter, D. Ron, The unfolded protein response: From stress pathway to homeostatic regulation. *Science* **334**, 1081–1086 (2011).
11. A. E. Frakes, A. Dillin, The UPR(ER): Sensor and coordinator of organismal homeostasis. *Mol. Cell* **66**, 761–771 (2017).

12. S. Song, J. Tan, Y. Miao, Q. Zhang, Crosstalk of ER stress-mediated autophagy and ER-phagy: Involvement of UPR and the core autophagy machinery. *J. Cell. Physiol.* **233**, 3867–3874 (2018).
13. M. Calfon, H. Zeng, F. Urano, J. H. Till, S. R. Hubbard, H. P. Harding, S. G. Clark, D. Ron, IRE1 couples endoplasmic reticulum load to secretory capacity by processing the XBP-1 mRNA. *Nature* **415**, 92–96 (2002).
14. B. Liu, H. Du, R. Rutkowski, A. Gartner, X. Wang, LAAT-1 is the lysosomal lysine/arginine transporter that maintains amino acid homeostasis. *Science* **337**, 351–354 (2012).
15. G. A. Wyant, M. Abu-Remaileh, R. L. Wolfson, W. W. Chen, E. Freinkman, L. V. Danai, M. G. Vander Heiden, D. M. Sabatini, mTORC1 activator SLC38A9 is required to efflux essential amino acids from lysosomes and use protein as a nutrient. *Cell* **171**, 642–654.e12 (2017).
16. S. Frølund, R. Holm, B. Brodin, C. Nielsen, The proton-coupled amino acid transporter, SLC36A1 (hPAT1), transports Gly-Gly, Gly-Sar and other Gly-Gly mimetics. *Br. J. Pharmacol.* **161**, 589–600 (2010).
17. A. A. Soukas, C. E. Carr, G. Ruvkun, Genetic regulation of Caenorhabditis elegans lysosome related organelle function. *PLOS Genet.* **9**, e1003908 (2013).
18. R. C. Taylor, A. Dillin, XBP-1 is a cell-nonautonomous regulator of stress resistance and longevity. *Cell* **153**, 1435–1447 (2013).
19. M. Hansen, D. C. Rubinsztein, D. W. Walker, Autophagy as a promoter of longevity: Insights from model organisms. *Nat. Rev. Mol. Cell Biol.* **19**, 579–593 (2018).
20. V. Olin-Sandoval, J. S. L. Yu, L. Miller-Fleming, M. T. Alam, S. Kamrad, C. Correia-Melo, R. Haas, J. Segal, D. A. Peña Navarro, L. Herrera-Dominguez, O. Méndez-Lucio, J. Vowinckel, M. Mülleder, M. Ralser, Lysine harvesting is an antioxidant strategy and triggers underground polyamine metabolism. *Nature* **572**, 249–253 (2019).
21. G. T. Hanson, R. Aggeler, D. Oglesbee, M. Cannon, R. A. Capaldi, R. Y. Tsien, S. J. Remington, Investigating mitochondrial redox potential with redox-sensitive green fluorescent protein indicators. *J. Biol. Chem.* **279**, 13044–13053 (2004).
22. C. T. Dooley, T. M. Dore, G. T. Hanson, W. C. Jackson, S. J. Remington, R. Y. Tsien, Imaging dynamic redox changes in mammalian cells with green fluorescent protein indicators. *J. Biol. Chem.* **279**, 22284–22293 (2004).
23. M. Li, Y. Rong, Y.-S. Chuang, D. Peng, S. D. Emr, Ubiquitin-dependent lysosomal membrane protein sorting and degradation. *Mol. Cell* **57**, 467–478 (2015).
24. K. M. Glover-Cutter, S. Lin, T. K. Blackwell, Integration of the unfolded protein and oxidative stress responses through SKN-1/Nrf. *PLOS Genet.* **9**, e1003701 (2013).
25. M. Forgac, Vacuolar ATPases: Rotary proton pumps in physiology and pathophysiology. *Nat. Rev. Mol. Cell Biol.* **8**, 917–929 (2007).
26. S.-K. Lee, W. Li, S.-E. Ryu, T. Rhim, J. Ahnn, Vacuolar (H+)-ATPases in Caenorhabditis elegans: What can we learn about giant H+ pumps from tiny worms? *Biochim. Biophys. Acta* **1797**, 1687–1695 (2010).
27. R. L. Wolfson, D. M. Sabatini, The dawn of the age of amino acid sensors for the mTORC1 pathway. *Cell Metab.* **26**, 301–309 (2017).
28. R. Zoncu, L. Bar-Peled, A. Efeyan, S. Wang, Y. Sancak, D. M. Sabatini, mTORC1 senses lysosomal amino acids through an inside-out mechanism that requires the vacuolar H(+)-ATPase. *Science* **334**, 678–683 (2011).
29. L. Bar-Peled, D. M. Sabatini, Regulation of mTORC1 by amino acids. *Trends Cell Biol.* **24**, 400–406 (2014).
30. L. Bar-Peled, L. D. Schweitzer, R. Zoncu, D. M. Sabatini, Ragulator is a GEF for the rag GTPases that signal amino acid levels to mTORC1. *Cell* **150**, 1196–1208 (2012).
31. Y. Sancak, L. Bar-Peled, R. Zoncu, A. L. Markhard, S. Nada, D. M. Sabatini, Ragulator-Rag complex targets mTORC1 to the lysosomal surface and is necessary for its activation by amino acids. *Cell* **141**, 290–303 (2010).
32. C. Sidrauski, D. Acosta-Alvear, A. Khoutorsky, P. Vedantham, B. R. Hearn, H. Li, K. Gamache, C. M. Gallagher, K. K.-H. Ang, C. Wilson, V. Okreglak, A. Ashkenazi, B. Hann, K. Nader, M. R. Arkin, A. R. Renslo, N. Sonenberg, P. Walter, Pharmacological brake-release of mRNA translation enhances cognitive memory. *eLife* **2**, e00498 (2013).
33. R. García-Navas, M. Munder, F. Mollinedo, Depletion of L-arginine induces autophagy as a cytoprotective response to endoplasmic reticulum stress in human T lymphocytes. *Autophagy* **8**, 1557–1576 (2012).
34. A. Jézégou, E. Llinares, C. Anne, S. Kieffer-Jaquinod, S. O'Regan, J. Aupetit, A. Chabli, C. Sagné, C. Debacker, B. Chadefaux-Vekemans, A. Journet, B. André, B. Gasnier, Heptahelical protein PQLC2 is a lysosomal cationic amino acid exporter underlying the action of cysteamine in cystinosis therapy. *Proc. Natl. Acad. Sci. U.S.A.* **109**, E3434–E3443 (2012).
35. M. Sanchez-Alvarez, M. A. del Pozo, C. Bakal, AKT-mTOR signaling modulates the dynamics of IRE1 RNAse activity by regulating ER-mitochondria contacts. *Sci. Rep.* **7**, 16497 (2017).
36. P. I. Merksamer, A. Trusina, F. R. Papa, Real-time redox measurements during endoplasmic reticulum stress reveal interlinked protein folding functions. *Cell* **135**, 933–947 (2008).
37. W. P. Voth, J. D. Richards, J. M. Shaw, D. J. Stillman, Yeast vectors for integration at the HO locus. *Nucleic Acids Res.* **29**, e59 (2001).
38. J. R. Daniele, D. J. Esping, G. Garcia, L. S. Parsons, E. A. Arriaga, A. Dillin, High-throughput characterization of region-specific mitochondrial function and morphology. *Sci. Rep.* **7**, 6749 (2017).
39. K. L. McDonald, R. I. Webb, Freeze substitution in 3 hours or less. *J. Microsc.* **243**, 227–233 (2011).
40. J. R. Daniele, R. Higuchi-Sanabria, J. Durieux, S. Monshietehadi, V. Ramachandran, S. U. Tronnes, N. Kelet, M. Sanchez, M. G. Metcalf, G. Garcia, P. A. Frankino, C. Benitez, M. Zeng, D. J. Esping, L. Joe, A. Dillin, UPRER promotes lipophagy independent of chaperones to extend life span. *Sci. Adv.* **6**, eaaz1441 (2020).

Acknowledgments: We thank M. E. Sanabria for considerable effort in quantification of Biosorter data. We are grateful to J. Paul in conceptual guidance of the project and to J. Durieux for all artwork. We thank all members of the Dillin and Zoncu lab for guidance and helpful comments on the manuscript. **Funding:** This work was supported by grant 1K99AG065200-01A1 through the National Institute of Aging (NIA) and the Glenn Foundation for Medical Research Postdoctoral Fellowship to R.H.-S., the Jane Coffin Childs Memorial Fund to K.S., 2019-A-023-FEL from Larry L. Hillblom Foundation Postdoc Fellowship to R.B.-Z., 5F31AG055326-03 from the NIA to C.N.S., 5F31AR070013-04 from the NIAMS to E.J.G., EDUC3-08399 from the California Institute for Regenerative Medicine to A.A.-J., T32AG000266-20A1 and F32AG065381 from the NIA to C.P., 1R35GM122589 from NIGMS and 1R33AG051047 from NIA to L.A.P., 1R01GM130995-01A1 and R01GM127763-01A1 from NIGMS to R.Z., and 5R01AG042679-02 through the NIA and the Howard Hughes Medical Institute to A.D. We thank the CGC funded by NIH Office of Research Infrastructure Programs P40 OD010440 for strains. **Author contributions:** R.H.-S. designed the project and experiments, prepared the manuscript and figures, and conducted experiments for all figures and supplemental figures. K.S. designed experiments, helped to write the manuscript, and performed experiments. N.K. performed experiments for Fig. 3 and figs. S1 to S4. R.B.-Z. and N.K. helped perform the screen. P.A.F. performed experiments for fig. S2. J.D. created all artwork. J.D. and S.M. performed life spans. S.H. and R.W. helped perform reporter imaging experiments. M.S. performed electron microscopy experiments. C.N.S., E.J.G., and L.A.P. performed *S. cerevisiae* experiments. L.J. and R.B.-Z. performed RNA-seq analysis. S.D., B.W., and S.U.T. performed critical experiments for developing the project. A.A.-J. performed screen follow-up experiments. C.P. performed motility assays. R.Z. and A.D. helped in developing the project and experiments, provided all resources, and assisted in manuscript preparation. **Competing interests:** The authors declare that they have no competing interests. **Data and materials availability:** All data needed to evaluate the conclusions in the paper are present in the paper and/or the Supplementary Materials. Raw RNA-seq datasets are available at Mendeley (DOI: 10.17632/grshntcjrb.2). Additional data related to this paper may be requested from the authors. All strains synthesized in this manuscript are derivatives of N2 or other strains from CGC and are either available on CGC or available upon request.

Submitted 25 October 2019
Accepted 13 May 2020
Published 26 June 2020
10.1126/sciadv.aaz9805

Citation: R. Higuchi-Sanabria, K. Shen, N. Kelet, P. A. Frankino, J. Durieux, R. Bar-Ziv, C. N. Sing, E. J. Garcia, S. Homentcovschi, M. Sanchez, R. Wu, S. U. Tronnes, L. Joe, B. Webster, A. Ahilon-Jeronimo, S. Monshietehadi, S. Dallarda, C. Pender, L. A. Pon, R. Zoncu, A. Dillin, Lysosomal recycling of amino acids affects ER quality control. *Sci. Adv.* **6**, eaaz9805 (2020).